Journal of Medicinal Chemistry

Drug Annotation

Discovery of 2-[[2-Ethyl-6-[4-[2-(3-hydroxyazetidin-1-yl)-2-oxo-ethyl]piperazin-1-yl]-8-methyl-imidazo[1,2-a]pyridin-3-yl]-methyl-amino]-4-(4-fluorophenyl)thiazole-5-carbonitrile (GLPG1690), a First-in-Class Autotaxin Inhibitor Undergoing Clinical Evaluation for the Treatment of Idiopathic Pulmonary Fibrosis

Nicolas Desroy, Christopher Housseman, Xavier Bock, Agnès Joncour, Natacha Bienvenu, Laëtitia Cherel, Virginie Labeguere, Emilie Rondet, Christophe Peixoto, Jean-Marie Joël Grassot, Olivier Picolet, Denis Annoot, Nicolas Triballeau, Alain Monjardet, Emanuelle Wakselman, Veronique Roncoroni, Sandrine Le Tallec, Roland Blanque, Celine Cottereaux, Nele Vandervoort, Thierry Christophe, Patrick Mollat, Marieke B. A. C. Lamers, Marielle Auberval, Boska Hrvacic, Jovica Ralic, Line Oste, Ellen Van der Aar, Reginald Brys, and Bertrand Heckmann

J. Med. Chem., **Just Accepted Manuscript** • DOI: 10.1021/acs.jmedchem.7b00032 • Publication Date (Web): 17 Apr 2017

Discovery of 2-[[2-Ethyl-6-[4-[2-(3-hydroxyazetidin-1-yl)-2-oxo-ethyl]piperazin-1-yl]-8-methyl-imidazo[1,2-a]pyridin-3-yl]-methyl-amino]-4-(4-fluorophenyl)thiazole-5-carbonitrile (GLPG1690), a First-in-Class Autotaxin Inhibitor Undergoing Clinical Evaluation for the Treatment of Idiopathic Pulmonary Fibrosis

Nicolas Desroy,[†,] Christopher Housseman,[†] Xavier Bock,[†] Agnès Joncour,[†] Natacha Bienvenu,[†] Laëtitia Cherel,[†] Virginie Labeguere,[†] Emilie Rondet,[†] Christophe Peixoto,[†] Jean-Marie Grassot,[†] Olivier Picolet,[†] Denis Annoot,[†] Nicolas Triballeau,[†] Alain Monjardet,[†] Emanuelle Wakselman,[†] Veronique Roncoroni,[†] Sandrine Le Tallec,[†] Roland Blanque,[†] Celine Cottereaux,[†] Nele Vandervoort,[‡] Thierry Christophe,[‡] Patrick Mollat,[†] Marieke Lamers,[○] Marielle Auberval,[†] Boska Hrvacic,[∥] Jovica Ralic,[∥] Line Oste,[‡] Ellen van der Aar,[‡] Reginald Brys[‡] and Bertrand Heckmann[†,*]*

[†]*Galapagos SASU, 102 avenue Gaston Roussel, 93230 Romainville, France*

[‡]*Galapagos NV, Generaal De Wittelaan L11 A3, 2800 Mechelen, Belgium*

[○]*Charles River Laboratories, Chesterford Research Park, CB10 1XL Saffron Walden, United Kingdom*

[‖]*Fidelta Ltd., Prilaz baruna Filipovića 29, Zagreb, HR-10000, Croatia*

ABSTRACT

Autotaxin is a circulating enzyme with a major role in the production of lysophosphatic acid (LPA) species in blood. A role for the autotaxin/LPA axis has been suggested in many disease areas including pulmonary fibrosis. Structural modifications of the known autotaxin inhibitor lead compound **1**, to attenuate hERG inhibition, remove CYP3A4 time-dependent inhibition and improve pharmacokinetic properties, led to the identification of clinical candidate GLPG1690 (**11**). Compound **11** was able to cause a sustained reduction of LPA levels in plasma *in vivo* and was shown to be efficacious in a bleomycin-induced pulmonary fibrosis model in mice, and in reducing extra-cellular matrix deposition in the lung whilst also reducing LPA 18:2 content in bronchoalveolar lavage fluid. Compound **11** is currently being evaluated in an exploratory phase 2a study in idiopathic pulmonary fibrosis patients.

INTRODUCTION

Autotaxin (ATX) is a secreted lysophophospholipase D (lysoPLD) that converts lysophosphatidyl choline (LPC) into the bioactive phospholipid derivative lysophosphatidic acid (LPA).[1] LPA consists of a glycerol backbone, a phosphate group and a fatty acyl chain of varying length and saturation (Figure 1). LPA exerts its biological activities through activation of

the LPA receptors: LPA_{1-6}.[2] The ATX/LPA axis has triggered considerable interest in the pharmaceutical industry due to its involvement in numerous physiological and pathophysiological processes.[3,4] A role for LPA and LPA receptors has been claimed in various pathologies such as cancer,[5] pain,[6] and cholestatic pruritus,[7] as well as fibrotic,[8] inflammatory,[9] and cardiovascular diseases.[10] We focused our research on lung diseases, more particularly on idiopathic pulmonary fibrosis (IPF). Several lines of evidence suggest that, by modulating the biology of lung epithelial cells, fibroblasts and smooth muscle cells, ATX/LPA signaling plays a role in various pulmonary diseases.[11,12] Studies related to IPF indicate an increase in LPA levels in the bronchoalveolar lavage fluid (BALF) of patients, as well as increased ATX levels in the lung.[11c,12c] Furthermore LPA_1 knock-out and inhibition studies revealed a key role for LPA in fibrotic processes in lung. These studies were then complemented by studies using knock-out mice lacking ATX expression specifically in bronchial epithelial cells and macrophages, in which these mice were shown to be less sensitive to experimental models of lung fibrosis.[11c] The role of LPA in lung remodeling relates to the effects of LPA on both lung fibroblasts (through LPA_1) and epithelial cells (through LPA_2). LPA_2 was shown to play a key role in the activation of TGF-β in epithelial cells under fibrotic conditions,[12c] and LPA_2 deficiency confers protection against bleomycin (BLM)-induced lung injury and fibrosis in mice.[12d] By inhibiting ATX mediated production of LPA, both LPA_1 and LPA_2 biology would be addressed suggesting an additional benefit compared to the use of LPA_1 or LPA_2 antagonists alone. In this article we will describe the discovery of **11** (GLPG1690),[13] a first in class ATX inhibitor currently evaluated in an exploratory phase 2a study in IPF patients.

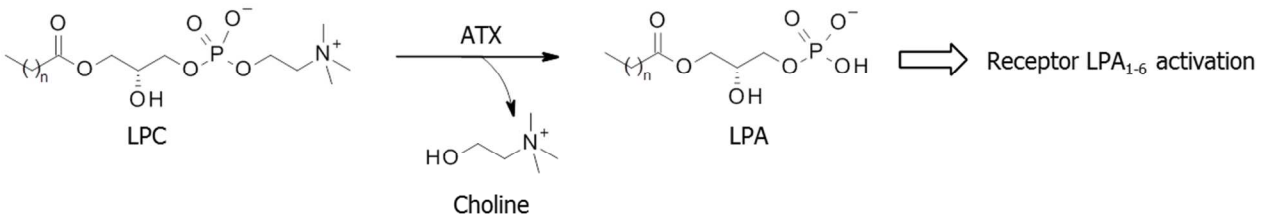

Figure 1. Conversion of LPC into LPA by ATX.

RESULTS AND DISCUSSION

HTS efforts identified 2,3,6 trisubstituted imidazo[1,2-a]pyridine derivatives as ATX inhibitors.[14] Subsequent structure-activity relationship exploration led to the identification of compound **1** as a potent ATX inhibitor in biochemical and rat plasma assays, with an IC_{50} of 27 nM and 22 nM respectively (Figure 2). However compound **1** showed limited oral exposure and unsatisfactory clearance in rodents. In addition compound **1** inhibited the hERG channel with an IC_{50} of 2.9μM in a hERG automated patch-clamp assay and showed CYP3A4 time-dependent inhibition (TDI) in a human liver microsomes assay (Table 1); these properties were not appropriate to initiate clinical development of compound **1**.

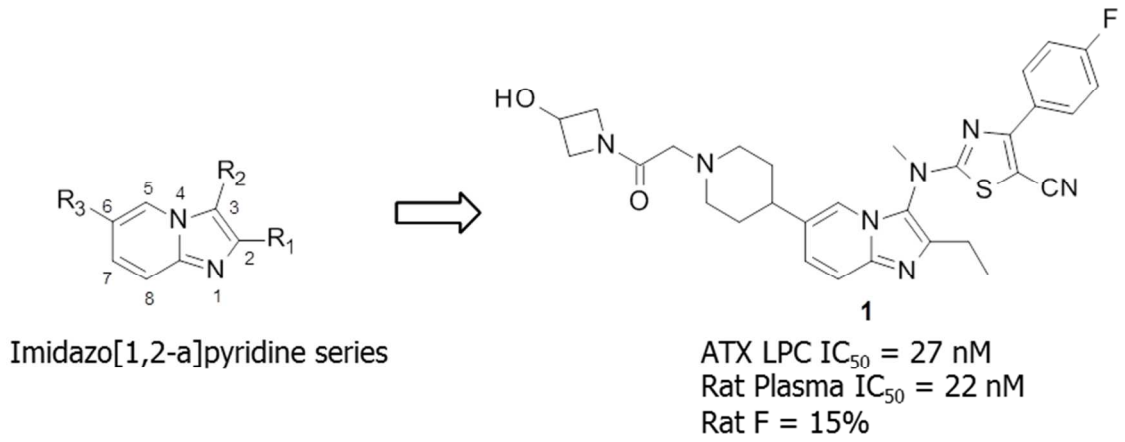

Figure 2. Hit series and Lead compound **1**.

We reasoned that hERG inhibition associated with compound **1** might be due to the presence of the basic piperidine linker (calculated pKa of 7.9). As seen in Table 1 replacement of the piperidine ring by a less basic piperazine ring at position 6 of the imidazo[1,2-a]pyridine scaffold for compounds **2** and **4** resulted in a lowering of hERG inhibition while retaining similar potency on ATX compared to compounds **1** and **3** respectively. However whereas hERG inhibition could be mitigated by lowering basicity, compounds **1-4** were positive in the CYP3A4 TDI assay in human liver microsomes. Variation of the substitution in position 6 of the imidazo[1,2-a]pyridine core had no impact on CYP3A4 TDI therefore scaffold modification was investigated.

Table 1. hERG inhibition and CYP3A4 TDI profiles

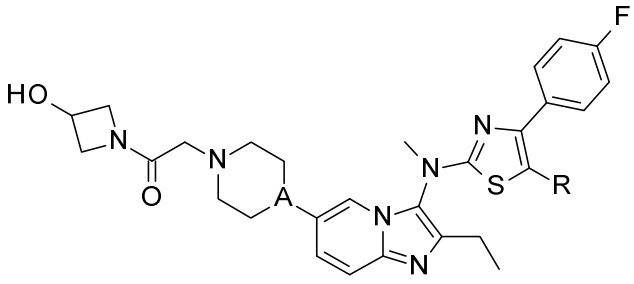

Compound	**Ring type** (A)	**R**	**ATX LPC** (IC_{50}, nM)	**hERG inhibition** (IC_{50}, μM)	**CYP3A4 TDI**	**Calculated pKa** [a]
1	Piperidine (CH)	CN	27	2.9	Positive	7.8
2	Piperazine (N)	CN	26	>11	Positive	5.9
3	Piperidine (CH)	H	246	5.6 [b]	Positive	7.8
4	Piperazine (N)	H	274	>33	Positive	5.9

[a] pKa calculation of conjugated acid on basic nitrogen of piperidine and piperazine rings performed with ACD/Labs Percepta Platform (2014). [b] data from hERG manual patch clamp assay.

As seen in Table 2, replacement of the imidazo[1,2-a]pyridine core in **2** with an imidazo[1,2-b]pyridazine backbone as in compound **5** led to comparable biochemical potency (27 nM vs 60 nM). In contrast replacement of the thiazole moiety by other heteroaromatic rings in position 3 as in compounds **6** and **7** led to 3 to 5 fold loss of potency versus **5**. Unfortunately exchanging the imidazo[1,2-a]pyridine scaffold for an imidazo[1,2-b]pyridazine ring in compound **5** had no impact on CYP3A4 TDI. Similarly the replacement of the thiazole ring by either a thiadiazole or a pyridine ring (as shown in compounds **6** and **7** respectively) also resulted in no impact. Remarkably, compound **8** bearing an imidazo[1,2-a]pyrazine scaffold displayed no CYP3A4 TDI. This marked improvement outweighed the 4-fold loss in activity of compound **8** versus **2**.

Table 2. CYP3A4 TDI profile of analogs of 2 with alternative scaffolds

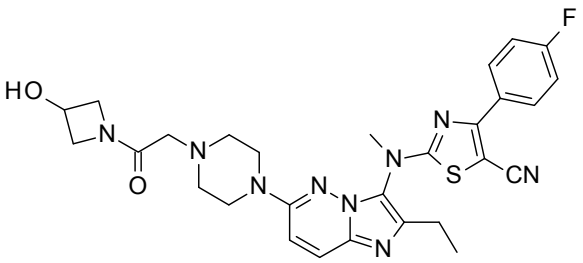

5

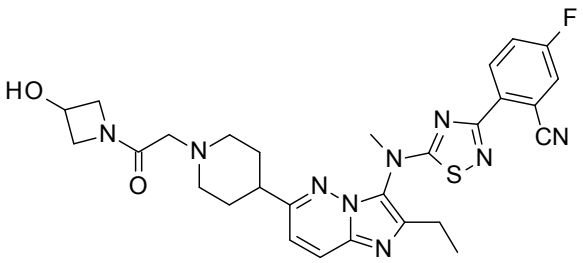

6

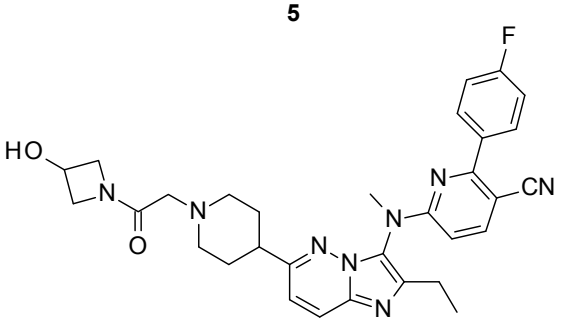

7

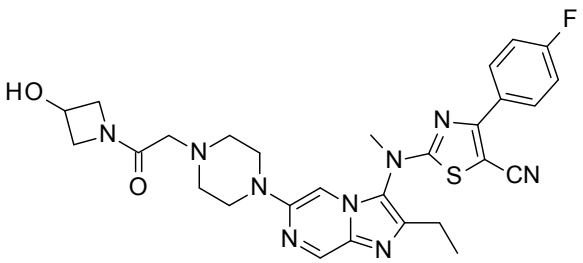

8

Compound	Scaffold	ATX LPC (IC_{50}, nM)	CYP3A4 TDI
5	Imidazo[1,2-b]pyridazine	60	Positive
6	Imidazo[1,2-b]pyridazine	297	Positive
7	Imidazo[1,2-b]pyridazine	192	Positive
8	Imidazo[1,2-a]pyrazine	102	Negative

When further derivatives with imidazo[1,2-a]pyrazine scaffold were prepared it appeared that DMSO solutions of compound **8** and analogs thereof degraded upon storage. This chemical instability prevented further progression of derivatives with this core. ^{1}H NMR and LCMS analysis of DMSO stock solutions of **8** and analogs suggested that oxidation of the imidazo[1,2-a]pyrazine scaffold might occur, although the degradants were not isolated. The absence of CYP3A4 TDI for compound **8** indicated the C_7-C_8 double bond of the imidazo[1,2-a]pyridine or imidazo[1,2-b]pyridazine scaffolds might be responsible for the occurrence of CYP3A4 TDI for compounds **1**-**7**. As can be seen in Scheme 1, putative metabolic oxidation of the C_7-C_8 double bond of the imidazo[1,2-a]pyridine ring leads to a reactive epoxide metabolite that can be trapped by glutathione (GSH) or nucleophilic residues in CYPs.[15] Steric hindrance caused by a methyl group on the C_7 or C_8 position of the imidazo[1,2-a]pyridine scaffold presumably disfavored this oxidative pathway in compounds **9** and **10**, which displayed no CYP3A4 TDI liability (Table 3). However introduction of the methyl substituent led to a 3 to 4-fold loss of potency in the biochemical assay compared to **1** and **3** respectively.

Scheme 1. Formation and trapping of reactive metabolite on imidazo[1,2-a]pyridine scaffold

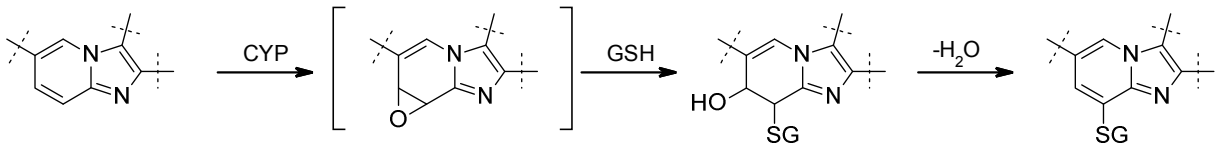

Table 3. Biochemical activity and CYP3A4 TDI profile of compounds 1, 3, 9, 10

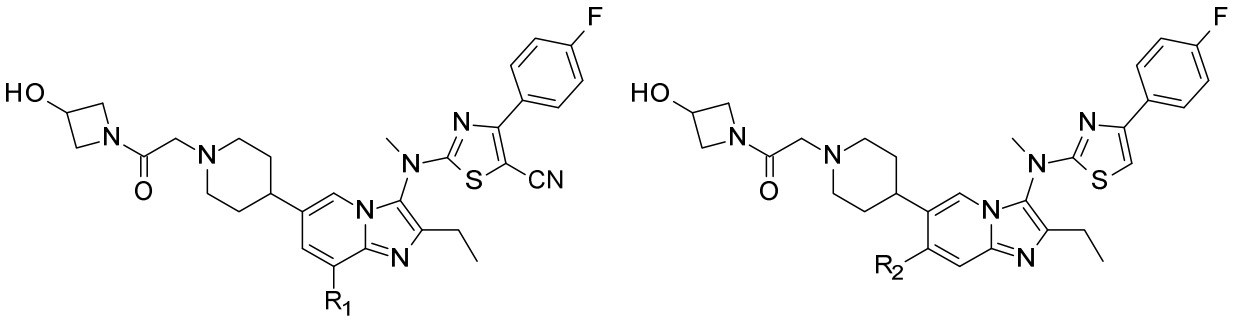

Compound	**1**	**9**	**3**	**10**
R_1 or R_2	R_1=H	R_1=Me	R_2=H	R_2=Me
CYP3A4 TDI	positive	negative	positive	negative
ATX LPC (IC_{50}, nM)	27	103	246	811

Introduction of the methyl group on C_8 of the imidazo[1,2-a]pyridine was combined with the piperazine linker at C_6 to yield compound **11** (Figure 3). Compound **11** represented the optimum combination of structural features to achieve desired ADMET properties and ATX inhibitory activity. Several synthetic routes were envisaged for the preparation of compound **11**, in particular for the construction of the imidazo[1,2-a]pyridine core, which was usually prepared by 3-component Groebke-Blackburn-Bienaymé reaction using costly Walborsky's reagent. In order to prepare larger amounts of material and avoid limitations on reagent availability, an alternative

synthesis was developed from commercially available 5-bromo-3-methyl-pyridin-2-amine (Scheme 2). Multicomponent reaction with potassium cyanide, benzotriazole and propanal afforded the 3-amino imidazo[1,2-a]pyridine scaffold[16] that was formylated to give compound **12**. Methylation of **12** followed by deformylation led to intermediate **13**. The preformed anion of **13** reacted via nucleophilic aromatic substitution with **17**, which was synthesized by oxidative cyclization of 4-fluorobenzoylacetonitrile with thiourea[17] followed by Sandmeyer reaction. The brominated derivative **14** obtained underwent Buchwald coupling reaction with boc piperazine with subsequent removal of the protecting group to give intermediate **15**. Finally alkylation of **15** with the chloroacetamide derivative **18**, yielded compound **11** in 8 linear steps from 5-bromo-3-methyl-pyridin-2-amine.

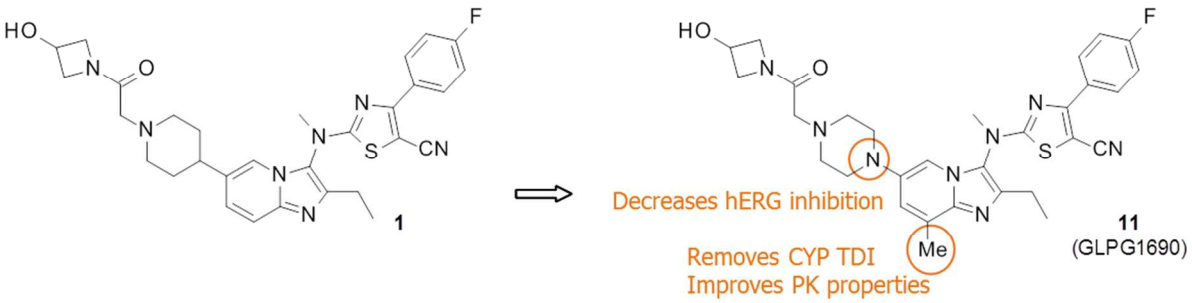

Figure 3. Structural modifications from **1** to **11**.

Scheme 2. Synthesis of **11**[a]

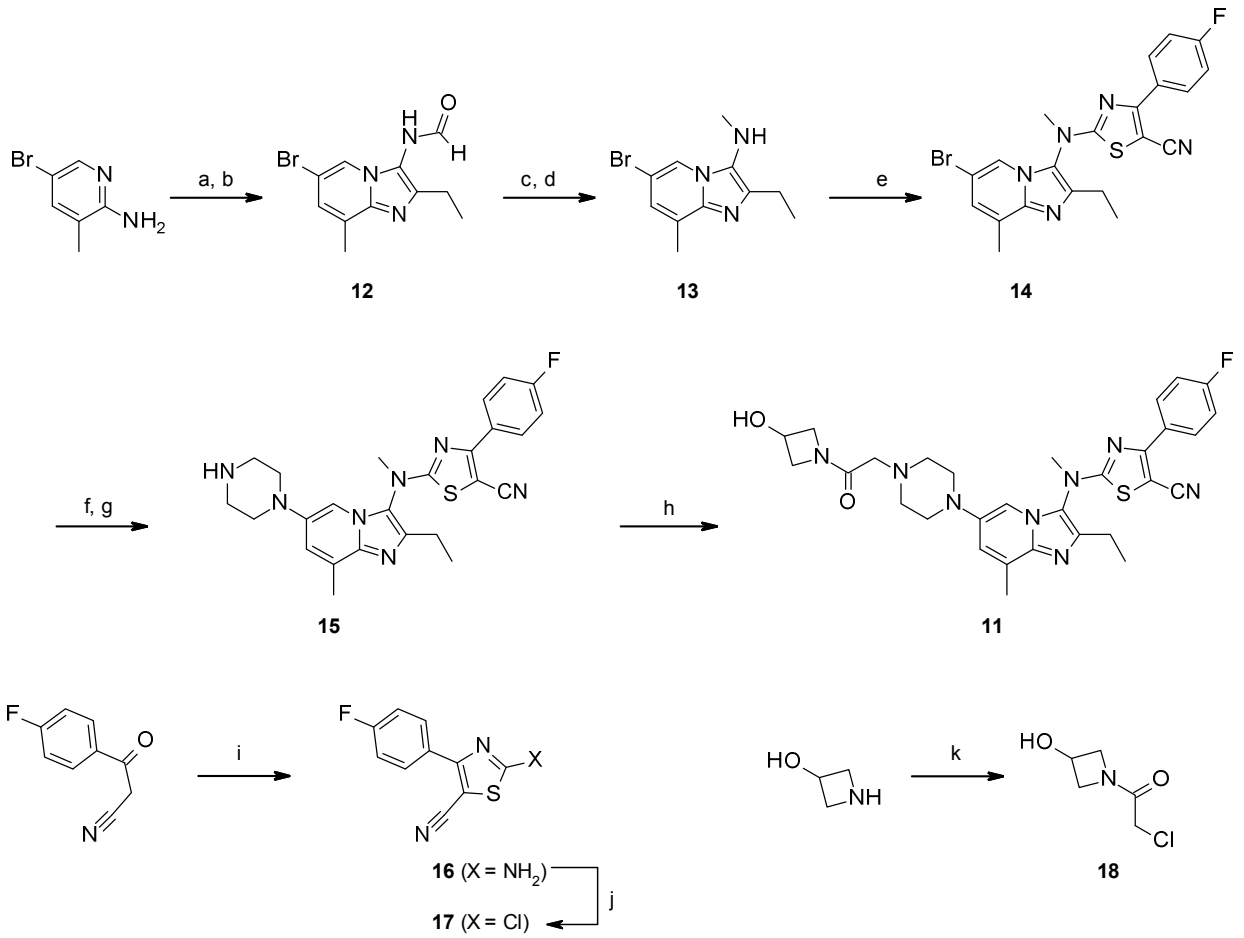

[a]Reagents and conditions: (a) (1) EtCHO, benzotriazole, toluene, rt then KCN, EtOH, rt to 80°C, (2) AcCl, EtOH, rt, 29%; (b) HCO_2H, 80°C, 95%; (c) K_2CO_3, MeI, acetone, 80°C, 93%; (d) HCl, MeOH, 80°C, 98%; (e) (1) NaH, THF, reflux, (2) **17**, 40°C to reflux, 73%; (f) boc-piperazine, tBuONa, Pd_2dba_3, JohnPhos, toluene, 115°C, 82%; (g) HCl, MeOH, rt, 90%; (h) **18**, K_2CO_3, MeCN, reflux, 81%; (i) pyridine, thiourea, iodine, EtOH, 70°C to rt, 65%; (j) $CuCl_2$, tBuONO, MeCN, rt, 62%; (k) Chloroacetyl chloride, K_2CO_3, H_2O, DCM, rt, 70%.

Compound **11** was co-crystallized with human ATX. Co-crystals diffracted with a maximum resolution of 2.4Å, enabling the construction of an experimental model of reasonably good quality (Rfree = 24.5%). Apart from a slight rotation of the core moiety of about 10°, compound **11** adopts the same binding mode as previously observed for the imidazo[1,2-a]pyridine derivative **19** (Figure 4A).[14] Introduction of the methyl group in position 8 of the imidazo[1,2-

a]pyridine core is deemed responsible for the positional shift which allows for a better fit in a locally constrained region of the protein. The three major substituents on the imidazo[1,2-a]pyridine core can be projected towards each of the 3 pockets of the T-shaped groove (Figure 4B). The short ethyl chain in position 2 of the imidazo[1,2-a]pyridine core points towards the catalytic site but remains remote from the reactive Thr210 (more than 5.7 Å for compound **11**, distance measured from the terminal methyl to the nucleophilic alcohol of Thr210). The 4-fluorophenyl-thiazole substituent in position 3 of the imidazo[1,2-a]pyridine core occupies the hydrophobic pocket and is positioned almost perpendicular to the imidazo[1,2-a]pyridine core via the N-methyl linker. The 4-fluorophenyl moiety makes an aromatic interaction (T-shape) with the side chain of Phe274. The nitrile group on the thiazole displaces a high energy water molecule leading to potency gain.[14] Finally, the substituted piperazine in position 6 of the imidazo[1,2-a]pyridine core lies in the hydrophobic channel. Some notable interactions in that region include a cation-pi interaction between the basic nitrogen of the piperazine and the indole side chain of Trp255 and a hydrogen bond between the carbonyl group of the acetyl chain on the piperazine and the indole NH of Trp261 possibly via a water molecule. Consequently the co-crystal structure of compound **11** in ATX shows the molecule occupies both the hydrophobic pocket, which otherwise accommodates the fatty acyl chain of LPA, and the hydrophobic channel, which is proposed to play a key role for the transport and delivery of LPA to its target receptors.[18] This particular binding mode could provide a significant advantage over other ATX inhibitors as it could prevent not only LPA formation but also ATX-mediated LPA delivery to its target receptors. As is highlighted in Figure 4, introduction of a methyl on the imidazo[1,2-a]pyridine core induces a scaffold rotation in order to fit within the protein. The requirement for

this positional shift possibly explains the slight activity loss observed for compound **11** versus the parent, non-methylated, analog **2** in the biochemical assay (IC_{50} of 131 nM versus 26 nM).

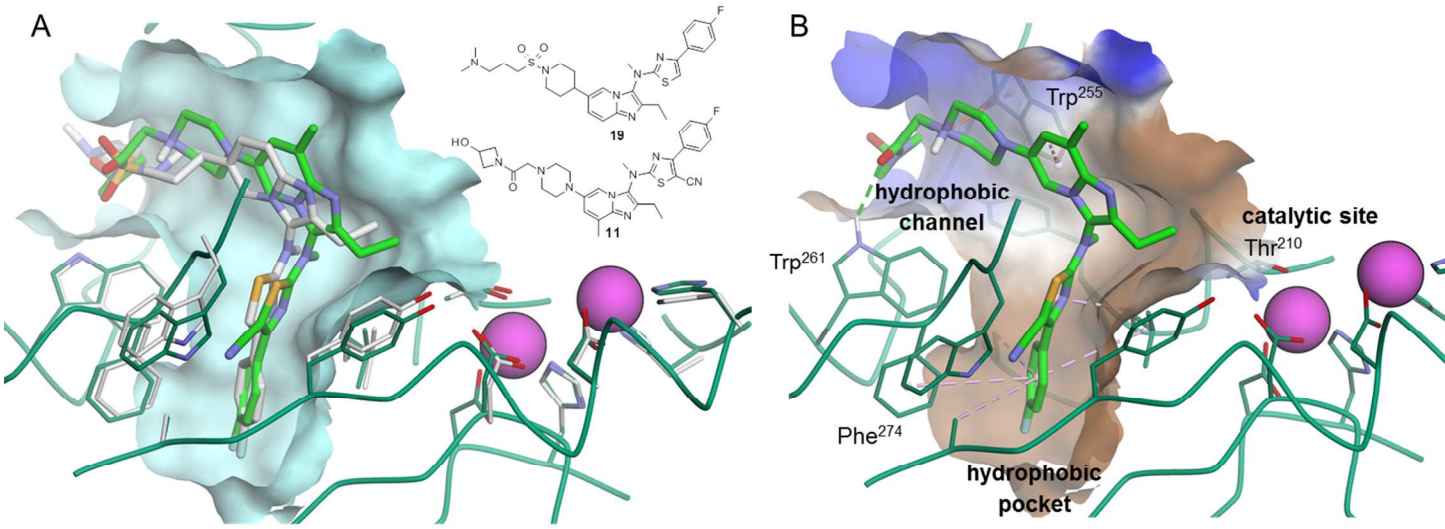

Figure 4. (A) Overlay of binding modes of compounds **11** (carbon atoms in light green) and **19** (carbon atoms in gray). The binding site carbon atoms and local backbone structures of ATX are depicted in dark green or gray. The two zinc atoms of the catalytic site are depicted in magenta in CPK mode. For clarity, the binding site surface has been clipped vertically. (B) Binding mode of compound **11** co-crystallized with human ATX. Protein-ligand interactions are represented by dashed lines (hydrogen bond in green, cation-pi interaction in orange and hydrophobic contacts in pink). The surface is colored by residue hydrophobicity (from brown for hydrophobic to blue for hydrophilic). For clarity, the surface has been clipped vertically.

Compound **11** was shown to inhibit ATX in a competitive manner versus the substrate (LPC) with a K_i of 15 nM (Table 4). Since ATX and LPC species are naturally present in plasma, the ability of compound **11** to inhibit the production of LPA in plasma from mice, rats or healthy

donors was evaluated by incubating plasma at 37°C for 2 h in the presence of a dose range of the compound. LPA 18:2 is one of the major LPA species present in plasma and was chosen as a representative species to monitor the reduction of LPA associated with ATX inhibition. The formation of LPA 18:2 was measured by LC-MS/MS using LPA 17:0 as a standard. Compound **11** inhibited ATX-induced LPA 18:2 production in mouse, rat and healthy donor plasma in a concentration-dependent manner, with IC_{50} values of 418 nM, 542 nM and 242 nM respectively. In view of the comparable high binding of compound **11** to plasma proteins in human and rodents (plasma protein binding higher than 99% was measured in human, dog, rat and mouse plasma), the observed inter-species difference in potency was considered as not significant. The high binding of compound **11** to plasma proteins does not seem to hamper the inhibition of ATX.

Table 4. Activity properties of compound 11

Compound	**11**
ATX LPC (IC_{50}, nM)	131
ATX LPC (K_i, nM)	15
Mouse plasma assay (IC_{50}, nM)	418
Rat plasma assay (IC_{50}, nM)	542
Human plasma assay (IC_{50}, nM)	242

With respect to ADMET properties compound **11** showed no CYP3A4 TDI and decreased hERG inhibitory activity (IC_{50} = 15 μM in manual patch clamp assay) compared to the lead compound **1** (Table 5). In addition, compound **11** displayed improved pharmacokinetic properties, with a lower plasma clearance and higher bioavailability than compound **1** in mouse and rat. The good

pharmacokinetic profile was further confirmed in dog, with compound **11** showing low plasma clearance (0.12 $L.h^{-1}.kg^{-1}$) and a high bioavailability (63%).

Table 5. In vitro properties and *in vivo* pharmacokinetic parameters for 1 and 11[a]

Compound	**1**	**11**
hERG inhibition (IC_{50}, μM)[b]	2.9 (APC)	15 (MPC)
CYP3A4 TDI	positive	negative
mouse i.v. Cl ($L\ h^{-1}\ kg^{-1}$)	1.2	0.23
mouse p.o. F (%)	12	29
rat i.v. Cl ($L\ h^{-1}\ kg^{-1}$)	3.1	0.69
rat p.o. F (%)	15	37
dog i.v. Cl ($L\ h^{-1}\ kg^{-1}$)	n.d.[c]	0.12
dog p.o. F (%)	n.d.[c]	63

[a]Mouse and rat oral bioavailability determined from 5 mg/kg p.o. (p.o. = per os) and 1 mg/kg i.v. (i.v. = intravenous) doses. Dog oral bioavailability determined from 1 mg/kg p.o. and i.v. doses. [b]APC: automated patch clamp assay, MPC: manual patch clamp assay. [c]n.d.: not determined.

In order to evaluate the PK/PD relationship for compound **11**, *in vivo* reduction of plasma LPA upon administration of compound **11** was monitored. Conversion of LPC into LPA by ATX is the major source of circulating LPA in blood.[1] *In vivo* inhibition of this process can be evaluated by quantification of LPA levels in plasma. Mice received a single dose of compound **11** (3, 10 or 30 mg/kg) under fasted conditions. Blood was sampled predose and 1, 3, 6 and 24 hours post-dosing for the determination of the levels of both compound **11** and LPA 18:2 (the biomarker) in plasma using LC-MS/MS. Mean plasma concentrations of **11** and mean percentage of LPA reduction are displayed in Figure 5. Mean pharmacokinetic parameters of **11** and the maximum reduction of LPA production are shown in Table 6. Following oral administration of compound

11 at 3, 10 and 30 mg/kg, prolonged absorption was seen, and a roughly dose-proportional increase of C_{max} and $AUC_{(0\text{-}24h)}$ were observed. As seen in Figure 5, the decrease in plasma LPA levels at 3, 10 and 30 mg/kg was concomitant with the increasing plasma concentration of compound **11**, thus demonstrating target engagement *in vivo* from a dose of 3 mg/kg onwards. At 3 mg/kg, compound **11** exposure in plasma covered the IC_{50} level, determined in the mouse plasma assay, for approximately 6 hours which resulted in at least 50% reduction of LPA levels for more than 6 hours. The higher compound exposure levels at 10 and 30 mg/kg led to a stronger and more sustained reduction of LPA levels. The peak of compound activity was detected at 3 hours post dosing whatever the dose, whereas t_{max} for compound **11** in plasma was reached between 1 and 3 hours post dosing depending on the dose. A maximal reduction in plasma LPA levels of 84%, 91% and 95% was achieved at 3, 10 and 30 mg/kg respectively.

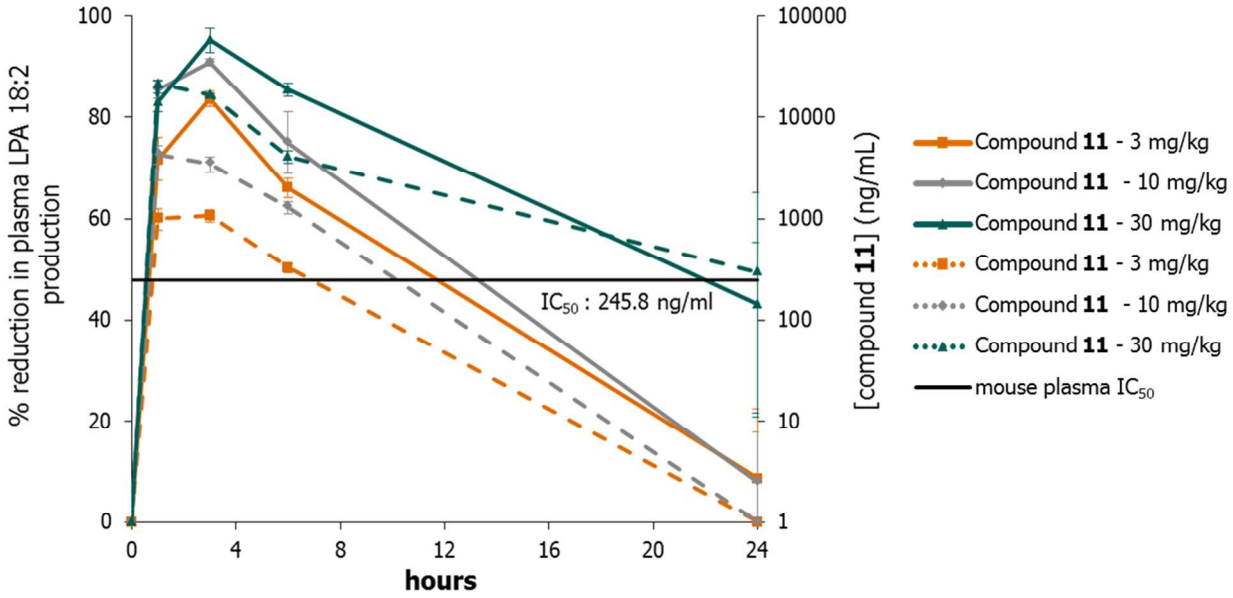

Figure 5. Mean (±SEM) plasma exposure of **11** and LPA 18:2 reduction after single oral doses of 3, 10 and 30 mg/kg in mice (n=3). Plasma exposure of **11** and LPA 18:2 reduction levels are

represented by dashed lines and solid lines respectively. The horizontal black line corresponds to the IC_{50} (ng/mL) of **11** determined in the mouse plasma assay.

Table 6. Pharmacokinetic parameters of 11 and *in vivo* LPA reduction[a]

	3 mg/kg p.o.	**10 mg/kg p.o.**	**30 mg/kg p.o.**
$\mathbf{C_{max}}$(ng/mL)	1,075	4,363	21,367
$\mathbf{C_{max}}$**/Dose**	358	436	712
$\mathbf{t_{max}}$(h)	3	1	1
$\mathbf{AUC_{(0\text{-}24h)}}$(ng.h/mL)	5,553	20,786	101,225
$\mathbf{AUC_{(0\text{-}24h)}}$**/Dose**	1,851	2,079	3,374
$\mathbf{C_{24h}}$(ng/mL)	1	4	295
$\mathbf{t_{1/2}}$(h)	2.21	2.22	3.79
Max of LPA reduction	83.6%	90.9%	95.2%
Time at maximum reduction (h)	3	3	3

[a]Mean pharmacokinetic parameters and mean percentage of LPA 18:2 reduction in mouse plasma following a single oral administration of **11** in mice, at 3, 10 and 30 mg/kg (n=3).

As the BLM-induced pulmonary fibrosis model in rodents is the most commonly used animal model to investigate the potential of compounds as novel therapies for IPF,[19] the next step was the evaluation of the efficacy of compound **11** in a 21-day model of BLM-induced pulmonary fibrosis in mice. Compound **11** was evaluated in a prophylactic setting in comparison with the reference substance pirfenidone, an approved treatment for IPF patients with anti-fibrotic and anti-inflammatory effects.[20] An intranasal challenge of BLM was administered to mice, and oral treatment with pirfenidone (50 mg/kg) or compound **11** (10 or 30 mg/kg), twice a day, started

simultaneously for 21 days. The efficacy of compound **11** and pirfenidone were evaluated based on the assessment of histopathological changes in lung architecture using Matsuse's modification of the Ashcroft score.[21] Intranasal application of BLM induced diffuse epithelial damage, pulmonary inflammation, fibrosis and occasionally severe focal distortion of the pulmonary structure, as observed in the vehicle control group. Within 21 days, the reference substance pirfenidone significantly reduced the Ashcroft score as compared to the vehicle-treated group (Figure 6). Treatment with compound **11** at a dose of 10 mg/kg or 30 mg/kg twice a day resulted in a significant reduction of the Ashcroft score. These effects were also reflected by lung weight measurements (data not shown). In addition, the efficacy of compound **11** given at 30 mg/kg twice a day was significantly better than that of pirfenidone based on the Ashcroft score.

The impact of compound **11** on LPA production in BALF was evaluated in the same BLM-induced pulmonary fibrosis mouse model. After 21 days, LPA 18:2 content in the BALF of mice challenged with PBS or BLM and treated with vehicle or compound **11** (30 mg/kg) was quantified by LC-MS/MS analysis. As can be seen in Figure 7, LPA 18:2 levels were significantly increased in the BLM group versus PBS-challenged animals and administration of compound **11** twice daily at 30 mg/kg resulted in a significant reduction of the LPA 18:2 BALF content in comparison to the diseased vehicle-treated group.[22] This result clearly demonstrated the ability of compound **11** to inhibit ATX mediated production of LPA 18:2 in BALF.

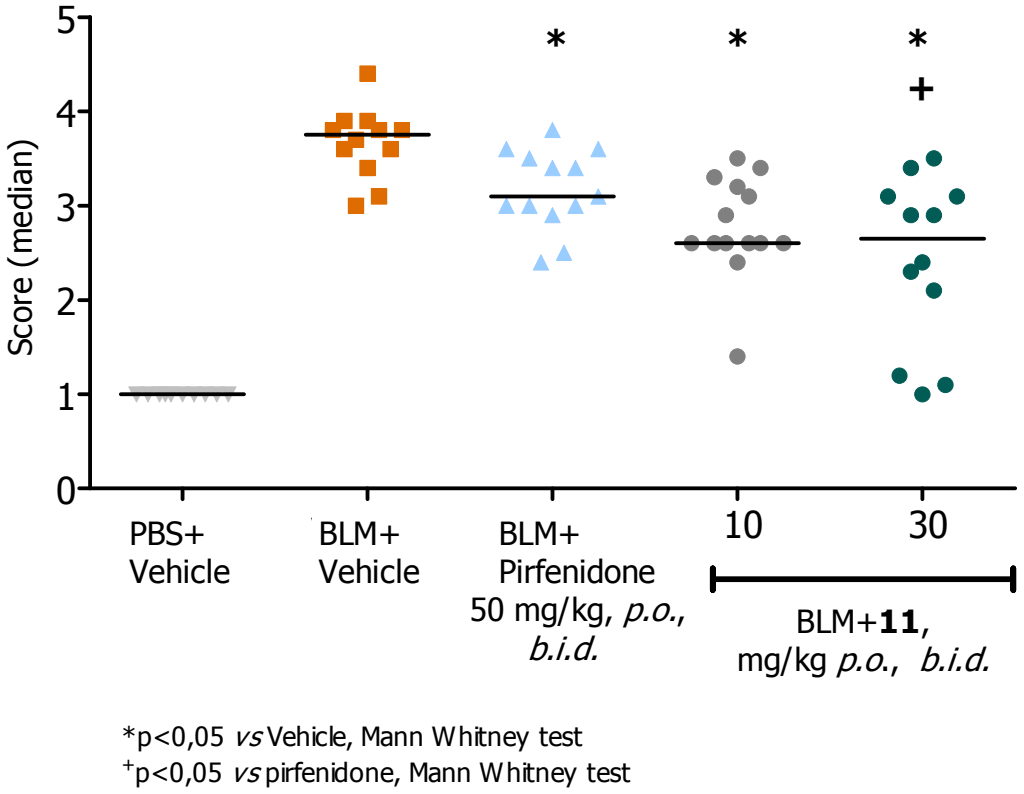

Figure 6. Activity of compounds in mouse BLM model: Ashcroft score (Matsuse's modification) at day 21. The efficacy of pirfenidone and compound **11** was compared to that of PBS-challenged and BLM-challenged groups that received vehicle as treatment. Total score for each animal was calculated as mean of the score obtained for ten low-power fields selected from the whole pulmonary area. Data are represented as group median. *p<0.05 *vs.* BLM-vehicle control; $^{+}$p<0.05 *vs.* BLM-pirfenidone; non-parametric Mann Whitney test.

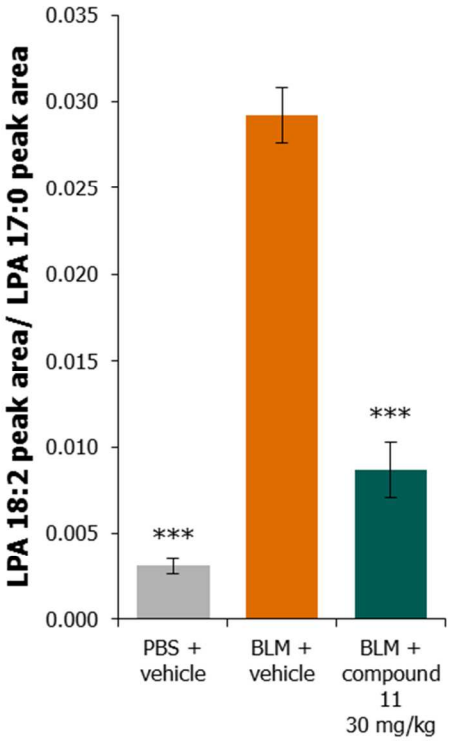

Figure 7. Analysis of LPA 18:2 in BALF of PBS-challenged mice (n=9) or BLM-challenged mice treated either with vehicle (n=6) or compound **11** (30 mg/kg twice daily, n=7) for 21 days. BALF was collected 2 hours after administration of either vehicle or compound **11**. Mean ± sem, ***p<0.001 *versus* BLM-vehicle by one-way ANOVA followed by Dunnett's multiple comparisons test.

CONCLUSION

The evolution of the potent autotaxin inhibitor lead compound **1** into clinical candidate **11** was achieved by appropriate structural modifications to improve ADMET (hERG and CYP3A4 TDI) and PK properties (bioavailability and clearance). Compound **11** was able to decrease LPA levels in a sustainable manner, in mouse plasma, from a dose of 3 mg/kg onwards. In addition, compound **11** demonstrated significant activity in the mouse BLM-induced fibrosis model at

doses of 10 and 30 mg/kg twice a day, with an efficacy comparable or superior to that of the reference compound pirfenidone. Compound **11** is currently being evaluated in an exploratory phase 2a study in IPF patients. Additional safety, pharmacological, pharmacokinetic and clinical data will be reported in due course.

EXPERIMENTAL SECTION

All reagents were of commercial grade and were used as received without further purification, unless otherwise stated. Commercially available anhydrous solvents were used for reactions conducted under inert atmosphere. Reagent grade solvents were used in all other cases, unless otherwise specified. Column chromatography was performed on silica gel 60 (35-70 μm). Thin layer chromatography was carried out using pre-coated silica gel F-254 plates (thickness 0.25 mm). Microwave heating was performed with a Biotage Initiator apparatus. Celpure® P65 is a filtration aid, commercial product (CAS number 61790-53-2). ^{1}H NMR spectra were recorded on a Bruker DPX 400 NMR spectrometer (400 MHz) or a Bruker Advance 300 NMR spectrometer (300 MHz). Chemical shifts (δ) for ^{1}H NMR spectra are reported in parts per million (ppm) relative to tetramethylsilane (δ 0.00) or the appropriate residual solvent peak, i.e. $CHCl_3$ (δ 7.27), as internal reference. Multiplicities are given as singlet (s), doublet (d), triplet (t), quartet (q), quintuplet (quin), multiplet (m) and broad (br). Waters Acquity UPLC with Waters Acquity PDA detector and SQD mass spectrometer was used to generate UV and MS chromatograms as well as MS spectra. Columns used: UPLC BEH C18 1.7 μm 2.1 x 5 mm VanGuard Pre-column with Acquity UPLC BEH C18 1.7 μm 2.1 x 30 mm column or Acquity UPLC BEH C18 1.7 μm 2.1 x 50 mm column. LC−MS analyses were conducted using the following two methods. Method 1:

solvent A, H_2O−0.05% NH_4OH; solvent B, MeCN−0.05% NH_4OH; flow rate, 0.8 mL/min; start 5% B, final 95% B in 1.55 min, linear gradient. Method 2: solvent A, H_2O−0.1% HCO_2H; solvent B, MeCN−0.1% HCO_2H; flow rate, 0.8 mL/min; start 5% B, final 95% B in 1.55 min, linear gradient. All final compounds reported were analyzed using one of these analytical methods and were at least 95% pure. Autopurification system from Waters was used for LC-MS purification. LC-MS columns used: Waters XBridge Prep OBD C18 5 μm 30 × 100 mm (preparative column) and Waters XBridge BEH C18 5 μm 4.6 × 100 mm (analytical column). All the methods used MeCN/H_2O gradients. MeCN and H_2O contained either 0.1% formic acid or 0.1% diethylamine. API5500 QTRAP mass spectrometer from ABSciex was used for the detection and quantification of compound and LPA in plasma. The hERG automated and manual patch clamp assays were performed at BioFocus (now Charles River Laboratories). The CYP3A4 TDI assay in human liver microsomes was performed at Fidelta and BioFocus; compounds were evaluated using testosterone and midazolam as probe substrates. A compound was considered positive in the CYP3A4 TDI assay when the IC_{50} shift between with and without pre-incubation conditions was higher than 2 fold. When IC_{50} could not be determined for both conditions, the compound was considered positive when sigmoidal curves would show misalignment. The BLM-induced pulmonary fibrosis model in mice was performed at Fidelta. Biochemical and plasma assays, preparation of compound **18**, protein production and purification will be described separately.[14]

2-[[2-Ethyl-6-[4-[2-(3-hydroxyazetidin-1-yl)-2-oxo-ethyl]piperazin-1-yl]-8-methyl-imidazo[1,2-a]pyridin-3-yl]-methyl-amino]-4-(4-fluorophenyl)thiazole-5-carbonitrile (11).

To a solution of 2-[(2-ethyl-8-methyl-6-piperazin-1-yl-imidazo[1,2-a]pyridin-3-yl)-methyl-amino]-4-(4-fluorophenyl)thiazole-5-carbonitrile (**15**) (18.05 g, 38 mmol) in MeCN (126 mL)

were added potassium carbonate (10.49 g, 75.9 mmol) and 2-chloro-1-(3-hydroxyazetidin-1-yl)ethanone (**18**) (7.38 g, 49.3 mmol). The reaction mixture was refluxed for 3.5 h then filtered and the solid was washed with MTBE and MeCN. The collected precipitate was then suspended in 300 mL of water, stirred for 1 h, filtered, and finally washed with water. The solid obtained was dried *in vacuo* to afford 2-[[2-ethyl-6-[4-[2-(3-hydroxyazetidin-1-yl)-2-oxo-ethyl]piperazin-1-yl]-8-methyl-imidazo[1,2-a]pyridin-3-yl]-methyl-amino]-4-(4-fluorophenyl)thiazole-5-carbonitrile (**11**) (18.0 g, 81%). ^{1}H NMR (400 MHz, $CDCl_3$) δ ppm 8.20-8.12 (m, 2 H), 7.22-7.13 (m, 2 H), 6.99 (s, 2 H), 4.75-4.66 (m, 1 H), 4.51-4.43 (m, 1 H), 4.34-4.26 (m, 1 H), 4.14-4.05 (m, 1 H), 3.88 (dd, *J* = 10.9, 4.4 Hz, 1 H), 3.61 (s, 3 H), 3.14-3.02 (m, 6 H), 2.74 (q, *J* = 7.7 Hz, 2 H), 2.70-2.62 (m, 4 H), 2.59 (s, 3 H), 1.33 (t, *J* = 7.6 Hz, 3 H). LC-MS: m/z = 589.6 [M+H].

N-(6-Bromo-2-ethyl-8-methyl-imidazo[1,2-a]pyridin-3-yl)formamide (12). (a) To a suspension of 2-amino-5-bromo-3-methylpyridine (420 g, 2.24 mol, washed before use with an aqueous saturated $NaHCO_3$ solution) in toluene (1.5 L) under nitrogen atmosphere were added propanal (248 mL, 3.36 mol) and benzotriazole (281 g, 2.36 mol). The resulting mixture was stirred 4 h at room temperature. Then ethanol (3.5 L) and potassium cyanide (175 g, 2.70 mol) were added. ***CAUTION!*** *Potassium cyanide is highly toxic.* The reaction mixture was further stirred overnight at room temperature and refluxed for 2 h. After cooling to room temperature, the mixture was quenched by addition of a 2.5M NaOH aqueous solution (3 L). This experiment was performed in four batches with the same quantities of reagents, the crude mixtures were then pooled together and concentrated *in vacuo* to low volume. The remaining oil was diluted with EtOAc (15 L) and washed with a 2M NaOH aqueous solution (2 x 2 L). The aqueous layer was extracted twice with EtOAc (2 x 1 L). The combined organic layers were then dried over

Na_2SO_4, filtered and concentrated *in vacuo*. The crude mixture was dissolved in ethanol (2 L) and carefully added to a solution of acetyl chloride (1 L, 14.0 mol, 1.6 eq.) in ethanol (6 L). The resulting reaction mixture was stirred at room temperature overnight and then concentrated to dryness. The residue was triturated in DCM (7 L) for 3 days, the precipitate formed was collected, washed with DCM (2 x 500 mL) and dried to afford 6-bromo-2-ethyl-8-methylimidazo[1,2-a]pyridin-3-amine as a hydrochloride salt (791g, 29%). ^{1}H NMR (400 MHz, DMSO-d_6) δ (ppm) 8.70 (s, 1 H), 7.75 (s, 1 H), 4.86 (br s, 3 H), 2.81 (q, J = 7.6 Hz, 2 H), 2.56 (s, 3 H), 1.25 (t, J = 7.6 Hz, 3 H). LC-MS: m/z = 254.0/256.0 [M+H].

(b) A suspension of 6-bromo-2-ethyl-8-methylimidazo[1,2-a]pyridin-3-amine as a hydrochloride salt (785 g, 2.70 mol) in formic acid (713 mL) was heated at 80°C for 2 h. The crude mixture was concentrated *in vacuo* to low volume (about 400 mL). The residue was brought up in water (1 L) and a 3 M solution of NaOH (2 L), then further basified with a saturated $NaHCO_3$ solution until foaming ceased and pH reached 8-9. After homogenization for 1 h, the precipitate was filtered, washed with water (2 x 300 mL), then dissolved in a mixture of toluene and MeOH 3:1 (4 L) followed by concentration *in vacuo*. Trituration of the residue in a mixture of 200 mL of MeOH and 5 L of diisopropyl ether, decantation and filtration of the resulting suspension afforded N-(6-bromo-2-ethyl-8-methyl-imidazo[1,2-a]pyridin-3-yl)formamide (**12**) (724 g, 95%). ^{1}H NMR (400 MHz, DMSO-d_6), presence of 2 rotamers, δ (ppm) 10.2 (br s, 1 H), 8.51 (s, 1 H, one rotamer), 8.36 (s, 1 H, one rotamer), 8.23 (s, 1 H, one rotamer), 8.11 (s, 1 H), 7.23 (s, 1 H, one rotamer), 7.21 (s, 1 H, one rotamer), 2.63-2.60 (m, 2 H), 2.58 (s, 3 H, one rotamer), 2.56 (s, 3 H, one rotamer), 1.24-1.17 (m, 3 H). LC-MS: m/z = 282.0/284.0 [M+H].

6-Bromo-2-ethyl-N,8-dimethyl-imidazo[1,2-a]pyridin-3-amine (13). (a) To a suspension of N-(6-bromo-2-ethyl-8-methyl-imidazo[1,2-a]pyridin-3-yl)formamide (78.2 g, 277 mmol) and potassium carbonate (114.8 g, 831 mmol) in acetone (923 mL), iodomethane (25.9 mL, 416 mmol) was added at room temperature and the reaction mixture was stirred at 80°C overnight. The solids were filtered off and rinsed with acetone and DCM. The filtrate was concentrated and the obtained solid was triturated in Et_2O, filtered and rinsed with Et_2O and water. The solid was collected and dried under vacuum to afford N-(6-bromo-2-ethyl-8-methyl-imidazo[1,2-a]pyridin-3-yl)-N-methyl-formamide as a white solid (75.9 g, 93%). ^{1}H NMR (400 MHz, $CDCl_3$), presence of 2 rotamers, δ (ppm) 8.49 (s, 1H, minor rotamer), 8.19 (s, 1 H, major rotamer), 7.78 (s, 1 H, major rotamer), 7.65 (s, 1 H, minor rotamer), 7.15 (s, 1 H, major rotamer), 7.08 (s, 1 H, minor rotamer), 3.36 (s, 3 H, minor rotamer), 3.24 (s, 3 H, major rotamer), 2.73-2.70 (m, 2 H), 2.59 (s, 3 H), 1.31 (t, *J* = 7.6 Hz, 3 H). LC-MS: m/z = 296.0/298.0 [M+H].

(b) A solution of HCl 1.25 M in methanol (35 mL, 43.8 mmol) was added to N-(6-bromo-2-ethyl-8-methyl-imidazo[1,2-a]pyridin-3-yl)-N-methyl-formamide (5.0 g, 16.9 mmol) and the reaction mixture was stirred for 4 h at 80°C (oil bath temperature). Another addition of HCl 1.25 M in methanol (14 mL, 17.5 mmol) was performed and the reaction mixture was stirred at 80°C for 1 h then at 100°C overnight. Solvent was evaporated and the crude product was partitioned between water and DCM. The aqueous layer was basified with $NaHCO_3$ and extracted with DCM. Combined organic layers were washed with brine, dried over sodium sulfate, filtered and evaporated to give 6-bromo-2-ethyl-N,8-dimethyl-imidazo[1,2-a]pyridin-3-amine (**13**) (4.44 g, 98%) that was used in the next step without further purification. ^{1}H NMR (400 MHz, $CDCl_3$) δ ppm 8.05 (s, 1 H), 7.04 (s, 1 H), 2.84-2.78 (m, 5 H), 2.60 (s, 3 H), 1.35 (t, *J* = 7.6 Hz, 3 H). LC-MS: m/z = 268.2/270.3 [M+H].

2-[(6-Bromo-2-ethyl-8-methyl-imidazo[1,2-a]pyridin-3-yl)-methyl-amino]-4-(4-fluorophenyl)thiazole-5-carbonitrile (14). To a solution compound **13** (4.4 g, 16.6 mmol) in THF (44 mL) under argon was slowly added NaH (60% in oil suspension, 2.0 g, 50.0 mmol). The reaction mixture was heated at 90°C (oil bath temperature) for 30 min then cooled to 40°C before adding 2-chloro-4-(4-fluorophenyl)thiazole-5-carbonitrile (**17**) (4.74 g, 19.9 mmol). The reaction mixture was stirred at 90°C overnight. After cooling to room temperature the mixture was slowly quenched by addition of water and then diluted with EtOAc. The organic layer was separated and the aqueous layer extracted with EtOAc. The combined organic layers were then washed with water and brine, dried over Na_2SO_4, filtered and concentrated *in vacuo*. The residue was triturated in Et_2O, filtered and washed with Et_2O and MeCN. Recrystallization was performed in MeCN (180 mL) to afford compound **14** as an orange solid (5.7g, 73%). ^{1}H NMR (400 MHz, $CDCl_3$) δ (ppm) 8.21-8.15 (m, 2 H), 7.82 (s, 1 H), 7.25-7.18 (m 3 H), 3.66 (s, 3 H), 2.85-2.76 (m, 2 H), 2.68 (s, 3 H), 1.38 (t, J = 7.6 Hz, 3 H). LC-MS: m/z = 470.3/472.3 [M+H].

2-[(2-Ethyl-8-methyl-6-piperazin-1-yl-imidazo[1,2-a]pyridin-3-yl)-methyl-amino]-4-(4-fluorophenyl)thiazole-5-carbonitrile (15). (a) To a solution of compound **14** (24.2 g, 51.5 mmol) in toluene under argon were successively added N-boc-piperazine (14.4 g, 77.3 mmol), sodium *tert*-butoxide (9.9 g, 103 mmol), JohnPhos (1.54 g, 5.15 mmol) and $Pd_2(dba)_3$ (2.36 g, 2.58 mmol). The reaction mixture was heated at 115°C for 1 h. After cooling to room temperature, the reaction was filtered on Celpure® P65 and the filtrate was evaporated. The residue was dissolved in EtOAc and washed with water. The organic layer was further washed with brine, dried over Na_2SO_4, filtered and concentrated *in vacuo*. The crude product was purified by chromatography on silica gel to afford *tert*-butyl 4-[3-[[5-cyano-4-(4-fluorophenyl)thiazol-2-yl]-methyl-amino]-2-ethyl-8-methyl-imidazo[1,2-a]pyridin-6-

yl]piperazine-1-carboxylate (24.4 g, 82%). ^{1}H NMR (400 MHz, $CDCl_3$) δ (ppm) 8.18-8.14 (m, 2 H), 7.21-7.16 (m, 2 H), 7.08-7.02 (m, 2 H), 3.62 (s, 3 H), 3.61-3.57 (m, 4H), 3.07-2.96 (m, 4H), 2.80 (q, *J* = 7.6 Hz, 2 H), 2.66 (s, 3 H), 1.47 (s, 9 H), 1.36 (t, *J* = 7.6 Hz, 3 H). LC-MS: m/z = 576.6 [M+H].

(b) To a solution of the latter compound (24.4 g, 42.4 mmol) in MeOH (100 mL) was added a 2 M HCl solution in Et_2O (127 mL, 254 mmol). The reaction mixture was stirred at room temperature for 3.5 h then concentrated *in vacuo*. The residue was partitioned between EtOAc and water. The aqueous layer was extracted twice with EtOAc. A 2 M NaOH solution was added to the aqueous layer until pH 8-9 was reached and further extraction with EtOAc was performed. The combined organic layers were then washed with brine, dried over Na_2SO_4, filtered and concentrated *in vacuo*. The solid was stirred in heptane (100 mL) at room temperature overnight, filtered off, washed with heptane and Et_2O, and dried to afford 2-[(2-ethyl-8-methyl-6-piperazin-1-yl-imidazo[1,2-a]pyridin-3-yl)-methyl-amino]-4-(4-fluorophenyl)thiazole-5-carbonitrile (**15**) (18.06 g, 90%). ^{1}H NMR (400 MHz, $CDCl_3$) δ (ppm) 8.23-8.16 (m, 2 H), 7.24-7.16 (m, 2 H), 7.06-7.00 (m, 2 H), 3.61 (s, 3 H), 3.09-2.98 (m, 8 H), 2.75 (q, *J* = 7.6 Hz, 2 H), 2.61 (s, 3 H), 1.34 (t, *J* = 7.6 Hz, 3 H). LC-MS: m/z = 476.5 [M+H].

2-Amino-4-(4-fluorophenyl)thiazole-5-carbonitrile (16). To a solution of 4-fluorobenzoylacetonitrile (50 g, 306 mmol) in EtOH (600 mL) was added pyridine (24.7 mL, 306 mmol). The resulting mixture was stirred at 70°C for 15 min then cooled to room temperature. A previously stirred suspension of thiourea (46.7 g, 613 mmol) and iodine (77.8 g, 306 mmol) in EtOH (300 mL) was then slowly added. After 1 h at room temperature a cold 1 M $Na_2S_2O_3$ solution (360 mL) was added under stirring. The resulting precipitate was filtered, washed with water, and finally dried *in vacuo* to afford 2-amino-4-(4-fluoro-phenyl)-thiazole-5-

carbonitrile (**16**) as a white solid (22 g, 65%). ^{1}H NMR (400 MHz, DMSO-d_6) δ (ppm) 8.26 (s, 2 H), 7.99-7.94 (m, 2 H), 7.36 (t, J = 9.0 Hz, 2 H). LC-MS: m/z = 220.2 [M+H].

2-Chloro-4-(4-fluorophenyl)thiazole-5-carbonitrile (17). To a solution of copper (II) chloride (36.8 g, 273 mmol) in MeCN (500 mL) was added dropwise *tert*-butyl nitrite (40.7 mL, 342 mmol). After stirring at room temperature for 30 min, 2-amino-4-(4-fluorophenyl)thiazole-5-carbonitrile (50 g, 228 mmol) was introduced portionwise and stirring was continued for 1 h. The reaction mixture was then carefully quenched by addition of a 1 N HCl solution (750 mL). After 15 min stirring, the organic phase was separated; the aqueous phase was further extracted with EtOAc. The combined organic layers were washed with brine, dried over Na_2SO_4, filtered and concentrated *in vacuo*. The crude product was filtered on a silica plug (250 g) and eluted with DCM. Solvents were evaporated and the residue was finally triturated in heptane, filtered and dried to afford compound **17** (33.95 g, 62%). ^{1}H NMR (400 MHz, DMSO-d_6) δ (ppm) 8.10-8.03 (m, 2 H), 7.50-7.42 (m, 2 H). LC-MS: m/z = 239.2/241.3 [M+H].

Mouse PK/PD with compound 11. Female C57BL/6Rj mice, 4-5 weeks old (Janvier, Le Genest St Isle, France) were maintained in controlled environment and dosed with compound **11** formulated in PEG 200 / MC 0.5% (25 / 75; v / v) as a single oral gavage with a dose level of 3, 10 or 30 mg/kg (0.3, 1 or 3 mg/mL of **11** respectively). A control group received vehicle only. Blood samples were collected by intra-cardiac sampling under gaseous anaesthesia with isoflurane according to protocols approved by the GALAPAGOS Ethical Committee for animals welfare with the agreement of the Ministère de l'Enseignement Supérieur et de la Recherche and the Direction Départementale de la Protection des Populations, at the following time points: 1, 3, 6, 24 h after dosing and placed into tubes containing Li-heparin as anticoagulant. LPA 18:2 plasma peak areas and compound **11** plasma concentrations were assayed by LC-MS/MS.

Plasma concentrations of compound **11** were measured against a calibration curve consisting of eight levels with a 3-Log amplitude. Back-calculated values of the QCs (three levels prepared in duplicate) were used for accepting or rejecting the whole batch. The lower limit of quantification was 4 ng/mL for compound **11**, using a plasma volume of 25 µL. Plasma proteins were precipitated with an excess of methanol containing the internal standard and the corresponding supernatant was injected on a C18 column. Analytes were eluted out the HPLC system by increasing the percentage of the organic mobile phase. An API5500 QTRAP mass spectrometer (ABSciex™) was used for the detection and quantification of compound **11**. Pharmacokinetic parameters were calculated after averaging individual plasma concentrations, by non-compartmental analysis using WinNonlin® software (Pharsight, version 5.2): maximum plasma concentration, Cmax (ng/mL) with the corresponding time, t_{max} (h) for p.o. treatment; area under the plasma concentration versus time curve up to 24 h, $AUC_{(0\text{-}24\ h)}$ (ng.h/mL), calculated according to the log linear up/log down trapezoidal method; apparent terminal elimination half-life, $t_{1/2}$ (h) which was only reported if three or more time points were used for linear regression, and if r^2 >0.90. Plasma levels were compiled (average of the plasma levels of the 3 mice at each sampling time) and the corresponding plasma exposure-time profiles were plotted. Mean values may be below the limit of quantification. SEM were tabulated only if more than two values were above the limit of quantification.

For the analysis of LPA 18:2 plasma peak areas, plasma proteins from a 10 µL aliquot were precipitated with an excess of methanol containing the internal standard, LPA 17:0. After centrifugation, the corresponding supernatant was diluted and injected on a C18 column. Analytes were eluted out of the column under isocratic conditions. An API5500 QTRAP mass spectrometer (ABSciex™) was used for the detection of LPA 18:2. No calibration curve was

prepared for LPA 18:2 and all quantifications were performed based on peak area ratios (LPA 18:2 / LPA 17:0). LPA data were finally expressed as percentage of reduction (% reduction) using the formula: 100-[((LPA value at time point t)/(mean of LPA value at the same time point t, in vehicle group))*100].

Mouse 21-day BLM-induced pulmonary fibrosis model. An intranasal challenge of BLM, 30 µg/ 50 µL was administered to anesthetized C57Bl/6 male mice (Charles River, Italy), 11 weeks old at delivery. Control animals received a challenge of PBS. Pirfenidone formulated in 0.5% CMC was given by oral route at 50 mg/kg twice a day. Compound **11** was dissolved in PEG 200 / 0.5% MC (25 / 75, v / v) and orally administered at 10 or 30 mg/kg twice a day. The volume of administration was 10 mL/kg and a 7.5 h interval was observed between two daily dosings. Control groups received vehicle. Treatments started on day of intranasal instillations of BLM and were performed for 21 days. At initiation, 14 to 24 mice were allocated to the different groups. At necropsy, lungs were removed, weighed, formalin-fixed, paraffin-embedded *in toto* and stained according to Mallory method for connective tissue. The efficacy of compound **11** and pirfenidone was essentially evaluated via histopathological changes in lungs using Matsuse's modification of the Ashcroft score.[21] This score was defined as follows: 1 for normal tissue (no fibrosis), 2 for minimal fibrotic thickening of alveolar or bronchial walls (network of fine collagen fibrils), 3 for moderate fibrotic thickening of walls without obvious damage to lung architecture, 4 for fibrosis with damage of pulmonary structure (coarse fibrous bands or small fibrous masses, intra-alveolar collagen fibrils), 5 for large fibrous area with severe distortion of lung structure. Total score for each animal was calculated as mean of ten low-power fields covering whole pulmonary area. Statistical analysis was performed using group median and non-parametric Mann-Whitney test. In addition, broncho-alveolar lavages consisting in two

instillations of 0.5 mL ice cold saline were performed in satellite groups in order to assess LPA species concentration. BALF was collected 2 hours after administration of 30 mg/kg of compound **11**. LPA 18:2 was quantified by LC-MS/MS in the BALF of PBS + vehicle, BLM exposed and treated mice after 21 days of experiment.

AUTHOR INFORMATION

Corresponding Authors

*B.H.: phone, +33-1-4942-4700; e-mail, bertrand.heckmann@glpg.com

*N.D.: phone, +33-1-4942-4820; e-mail, nicolas.desroy@glpg.com

Notes

The authors declare the following competing financial interest(s): N. Desroy, C. Housseman, X. Bock, A. Joncour, N. Bienvenu, L. Cherel, V. Labeguere, C. Peixoto, O. Picolet, D. Annoot, N. Triballeau, A. Monjardet, E. Wakselman, V. Roncoroni, S. Le Tallec, R. Blanque, C. Cottereaux, P. Mollat, M. Auberval and B. Heckmann are employees of Galapagos SASU, France. N. Vandervoort, T. Christophe, L. Oste, E. van der Aar and R. Brys are employees of Galapagos NV, Belgium.

ACKNOWLEDGMENT

The authors thank Florence Bonnaterre for her contribution to the writing of the manuscript. Intermediate **12** was synthesized at Mercachem.

ABBREVIATIONS

ATX, autotaxin; BALF, bronchoalveolar lavage fluid; BLM, bleomycin; CYP3A4, cytochrome P450 3A4; Cl, clearance; hERG, human *ether-à-go-go*-related gene; IPF, idiopathic pulmonary fibrosis; i.v., intravenous; JohnPhos, (2-biphenyl)di-*tert*-butylphosphine; LC-MS, liquid chromatography mass spectrometry; LPA, Lysophosphatidic acid; LPC, Lysophosphatidyl choline; MC, methyl cellulose; PBS, phosphate-buffered saline; PEG, polyethylene glycol; p.o., *per os*; QC, quality control; $t_{1/2}$, half-life; TDI, time-dependent inhibition.

ASSOCIATED CONTENT

Supporting Information

Preparation and characterization for additional final compounds, Ki determination for compound **11,** co-crystallization protocol. This material is available free of charge via the Internet at http://pubs.acs.org.

Co-crystal structure of compound **11** with ATX (PDB ID: 5MHP): authors will release the atomic coordinates and experimental data upon article publication.

Molecular Formula Strings.

REFERENCES

(1) (a) Nakanaga, K.; Hama, K.; Aoki, J. Autotaxin-an LPA producing enzyme with diverse functions. *J. Biochem.* **2010**, *148*, 13-24. (b) Perrakis, A.; Moolenaar, W. H. Autotaxin: structure-function and signaling. *J. Lipid Res.* **2014**, *55*, 1010-1018.

(2) (a) Bandoh, K.; Aoki, J.; Taira, A.; Tsujimoto, M.; Arai, H.; Inoue, K. Lysophosphatidic acid (LPA) receptors of the EDG family are differentially activated by LPA species. *FEBS Lett.*

2000, *478*, 159-165. (b) Lin, M. E.; Herr, D. R.; Chun, J. Lysophosphatidic acid (LPA) receptors: Signaling properties and disease relevance. *Prostaglandins Other Lipid Mediators* **2010**, *91*, 130-138. (c) Stoddard, N. C.; Chun. J. Promising pharmacological directions in the world of lysophosphatidic acid signaling. *Biomol. Ther.* **2015**, 23, 1-11.

(3) Reviews: (a) Albers, H. M. H. G.; Ovaa, H. Chemical evolution of autotaxin inhibitors. *Chem. Rev.* **2012**, *112*, 2593-2603. (b) Barbayianni, E.; Magrioti, V.; Moutevelis-Minakakis, P.; Kokotos, G.; Autotaxin inhibitors: a patent review. *Expert Opin. Ther. Pat.* **2013**, *23*, 1123-1132. (c) Castagna, D.; Budd, D. C.; Macdonald S. J.; Jamieson C.; Watson A. J. Development of autotaxin inhibitors: an overview of the patent and primary literature. *J. Med. Chem.*, **2016**, *59*, 5604-5621.

(4) Recent reports of autotaxin inhibitors: (a) Kato, K.; Ikeda, H.; Miyakawa, S.; Futakawa, S.; Nonaka, Y.; Fujiwara, M.; Okudaira, S.; Kano, K.; Aoki, J.; Morita, J.; Ishitani, R.; Nishimasu, H.; Nakamura, Y.; Nureki, O. Structural basis for specific inhibition of autotaxin by a DNA aptamer. *Nat. Struct. Mol. Biol.* **2016**, *23*, 395-401. (b) Jones, S. B.; Pfeifer, L. A.; Bleisch, T. J.; Beauchamp, T. J.; Durbin, J. D.; Klimkowski, V. J.; Hughes, N. E.; Rito, C. J.; Dao, Y.; Gruber, J. M.; Bui, H.; Chambers, M. G.; Chandrasekhar, S.; Lin, C.; McCann, D. J.; Mudra, D. R.; Oskins, J. L.; Swearingen, C. A.; Thirunavukkarasu, K.; Norman, B. H. Novel autotaxin inhibitors for the treatment of osteoarthritis pain: lead optimization via structure-based drug design. *ACS Med. Chem. Lett.* **2016**, *7*, 857-861. (c) Shah, P.; Cheasty, A.; Foxton, C.; Raynham, T.; Farooq, M.; Gutierrez, I. F.; Lejeune, A.; Pritchard, M.; Turnbull, A.; Pang, L.; Owen, P.; Boyd, S.; Stowell, A.; Jordan, A.; Hamilton, N. M.; Hitchin, J. R.; Stockley, M.; MacDonald, E.; Quesada, M. J.; Trivier, E.; Skeete, J.; Ovaa, H.; Moolenaar, W. H.; Ryder, H. Discovery of

potent inhibitors of the lysophospholipase autotaxin. *Bioorg. Med. Chem. Lett.* **2016**, *26*, 5403-5410.

(5) (a) Mills, G. B.; Moolenaar, W. H. The emerging role of lysophosphatidic acid in cancer. *Nat. Rev. Cancer* **2003**, *3*, 582-591. (b) Leblanc, R.; Peyruchaud, O. New insights into the autotaxin/LPA axis in cancer development and metastasis. *Exp. Cell. Res.* **2015**, *333*, 183-189. (c) Benesch, M. G.; Ko, Y. M.; Mc Mullen, T. P.; Brindley, D. N. Autotaxin in the crosshairs: taking aim at cancer and other inflammatory conditions. *FEBS Lett.* **2014**, *588*, 2712-2727.

(6) (a) Inoue, M.; Rashid, M. H.; Fujita, R.; Contos, J. J. A.; Chun, J.; Ueda, H. Initiation of neuropathic pain requires lysophosphatidic acid receptor signaling. *Nat. Med.* **2004**, *10*, 712-714. (b) Thirunavukkarasu, K.; Swearingen, C. A.; Oskins, J. L.; Lin, C.; Bui, H. H.; Jones, S. B.; Pfeifer, L. A.; Norman, B. H.; Mitchell, P. G.; Chambers, M. G. Identification and pharmacological characterization of a novel inhibitor of autotaxin in rodent models of joint pain. *Osteoarthritis Cartilage.* [Online early access]. DOI: 10.1016/j.joca.2016.09.006. Published Online: September 13, 2016.

(7) (a) Kremer, A. E.; van Dijk, R.; Leckie, P.; Schaap, F. G.; Kuiper, E. M.; Mettang, T.; Reiners, K. S.; Raap, U.; van Buuren, H. R.; van Erpecum, K. J.; Davies, N. A.; Rust, C.; Engert, A.; Jalan, R.; Oude Elferink, R. P.; Beuers, U. Serum autotaxin is increased in pruritus of cholestasis, but not of other origin, and responds to therapeutic interventions. *Hepatology* **2012**, *56*, 1391-1400. (b) Wunsch, E.; Krawczyk, M.; Milkiewicz, M.; Trottier, J.; Barbier, O.; Neurath, M. F.; Lammert, F.; Kremer, A. E.; Milkiewicz, P. Serum autotaxin is a marker of the severity of liver injury and overall survival in patients with cholestatic liver diseases. *Sci. Rep.* [Online] **2016**, *6*, 30847; DOI: 10.1038/srep30847.

(8) (a) Bain, G.; Shannon, K. E.; Huang, F.; Darlington, J.; Goulet, L.; Prodanovich, P.; Ma, G. L.; Santini, A. M.; Stein, A. J.; Lonergan, D.; King, C. D.; Calderon, I.; Lai, A.; Hutchinson, J. H.; Evans, J. F. Selective inhibition of autotaxin is efficacious in mouse models of liver fibrosis. *J. Pharmacol. Exp. Ther.* [Online early access]. DOI: 10.1124/jpet.116.237156. Published Online: October 17, 2016. (b) Castelino, F. V.; Bain, G.; Pace, V. A.; Black, K. E.; George, L.; Probst, C. K.; Goulet, L.; Lafyatis, R.; Tager, A. M. An autotaxin/lysophosphatidic acid/interleukin-6 amplification loop drives scleroderma fibrosis. *Arthritis Rheumatol.* **2016**, *68*, 2964-2974.

(9) (a) Bourgion, S. G.; Zhao, C. Autotaxin and lysophospholipids in rheumatoid arthritis. *Curr. Opin. Invest. Drugs* **2010**, *11*, 515-526. (b) Park, G. Y.; Lee, Y. G.; Berdyshev, E.; Nyenhuis, S.; Du, J.; Fu, P.; Gorshkova, I. A.; Li, Y.; Chung, S.; Karpurapu, M.; Deng, J.; Ranjan, R.; Xiao, L.; Jaffe, H. A.; Corbridge, S. J.; Kelly, E. A.; Jarjour, N. N.; Chun, J.; Prestwich, G. D.; Kaffe, E.; Ninou, I.; Aidinis, V.; Morris, A. J.; Smyth, S. S.; Ackerman, S. J.; Natarajan, V.; Christman, J. W. Autotaxin production of lysophosphatidic acid mediates allergic asthmatic inflammation. *Am. J. Respir. Crit. Care Med.* **2013**, *188*, 928-940. (c) Zhao, Y.; Natarajan, V. Lysophosphatidic acid (LPA) and its receptors: Role in airway inflammation and remodeling. *Biochim. Biophys. Acta, Mol. Cell. Biol. Lipids* **2013**, *1831*, 86-92.

(10) Hui, D. Y. Intestinal phospholipid and lysophospholipid metabolism in cardiometabolic disease. *Curr. Opin. Lipidol.* **2016**, *27*, 507-512.

(11) (a) Budd, D. C.; Qian, Y. Development of lysophosphatidic acid pathway modulators as therapies for fibrosis. *Future Med. Chem.* **2013**, *5*, 1935-1952. (b) Chu, X.; Wei, X.; Lu, S.; He, P.; Autotaxin-LPA receptor axis in the pathogenesis of lung diseases. *Int. J. Clin. Exp. Med.*

2015, *8*, 17117-17122. (c) Oikonomou, N.; Mouratis, M. A.; Tzouvelekis, A.; Kaffe, E.; Valavanis, C.; Vilaras, G.; Karameris, A.; Prestwich, G. D.; Bouros, D.; Aidinis, V. Pulmonary autotaxin expression contributes to the pathogenesis of pulmonary fibrosis. *Am. J. Respir. Cell. Mol. Biol.* **2012**, *47*, 566-574.

(12) (a) Funke, M.; Zhao, Z.; Xu, Y.; Chun, J.; Tager, A. M. The lysophosphatidic acid receptor LPA1 promotes epithelial cell apoptosis after lung injury. *Am. J. Respir. Cell. Mol. Biol.* **2012**, *46*, 355-364. (b) Tager, A. M.; LaCamera, P.; Shea, B. S.; Campanella, G. S.; Selman, M.; Zhao, Z.; Polosukhin, V.; Wain, J.; Karimi-Shah, B. A.; Kim, N. D.; Hart, W. K.; Pardo, A.; Blackwell, T. S.; Xu, Y.; Chun, J.; Luster, A. D. The lysophosphatidic acid receptor LPA1 links pulmonary fibrosis to lung injury by mediating fibroblast recruitment and vascular leak. *Nat. Med.* **2008**, *14*, 45-54. (c) Xu, M. Y.; Porte, J.; Knox, A. J.; Weinreb, P. H.; Maher, T. M.; Violette, S. M.; McAnulty, R. J.; Sheppard, D.; Jenkins, G. Lysophosphatidic acid induces αvβ6 integrin-mediated TGF-β activation via the LPA2 receptor and the small G protein Gαq *Am. J. Pathol.* **2009**, 174, 1264-1279. (d) Huang, L. S.; Fu, P.; Patel, P.; Harijith, A.; Sun, T.; Zhao, Y.; Garcia, J. G.; Chun, J.; Natarajan, V. Lysophosphatidic acid receptor-2 deficiency confers protection against bleomycin-induced lung injury and fibrosis in mice. *Am. J. Respir. Cell. Mol. Biol.* **2013**, *49*, 912-922.

(13) (a) Desroy, N.; Heckmann, B.; Brys, R. C. X.; Joncour, A.; Peixoto, C.; Bock, X. Compounds and pharmaceutical compositions thereof for the treatment of inflammatory disorders. PCT Int. Appl. WO2014/139882 A1, 2014. (b) Desroy, N.; Joncour, A.; Bock, X.; Housseman, C.; Peixoto, C.; Bienvenu, N.; Labeguere, V.; Cherel, L.; Annoot, D.; Christophe, T.; Conrath, K.; Triballeau, N.; Mollat, P.; Wohlkonig, A.; Blanque, R.; Cottereaux, C.; Hrvacic, B.; Borgonovi, M.; Monjardet, A.; Van der Aar, E.; Brys, R.; Heckmann, B. Discovery of

GLPG1690: A first-in-class autotaxin inhibitor in clinical development for the treatment of idiopathic pulmonary fibrosis. *Abstracts of Papers, 251st ACS National Meeting & Exposition, San Diego, CA, United States, March 13-17, 2016,* MEDI-254.

(14) Manuscript in preparation.

(15) (a) Usui, T.; Mise, M.; Hashizume, T.; Yabuki, M.; Komuro, S. Evaluation of the potential for drug-induced liver injury based on in vitro covalent binding to human liver proteins. *Drug Metab. Dispos.* **2009**, *37*, 2383-2392. (b) Stepan, A. F.; Walker, D. P.; Bauman, J.; Price, D. A.; Baillie, T. A.; Kalgutkar, A. S.; Aleo, M. D. Structural alert/reactive metabolite concept as applied in medicinal chemistry to mitigate the risk of idiosyncratic drug toxicity: a perspective based on the critical examination of trends in the top 200 drugs marketed in the United States. *Chem. Res. Toxicol.* **2011**, *24*, 1345-1410.

(16) (a) Moutou, J.-L.; Schmitt, M.; Collot, V.; Bourguignon, J.-J. A two-steps benzotriazole-assisted synthesis of 3-amino-2-ethoxycarbonyl imidazo [1,2-a] pyridines and related compounds *Tetrahedron Lett.* **1996**, *37*, 1787-1790. (b) Katritzky, A. R.; Urogdi, L.; Mayence, A. The chemistry of *N*-substituted benzotriazoles Part 23. Synthesis of tertiary α-amino esters. *Synthesis* **1989**, 323-327.

(17) (a) Gonzalez Lio, L.; Camacho Gomez, J. A. New compounds as adenosine A1 receptor antagonists. PCT Int. Appl. WO2009044250 A1, 2009. (b) King, L. C.; Ryden, I. The reaction of ketones with formamidine disulfide. *J. Am. Chem. Soc.* **1947**, *69*, 1813-1814.

(18) (a) Moolenaar, W. H.; Perrakis, A. Insights into autotaxin: how to produce and present a lipid mediator. *Nat. Rev. Mol. Cell. Biol.* **2011**, *12*, 647-649. (b) Nishimasu, H.; Okudaira, S.; Hama, K.; Mihara, E.; Dohmae, N.; Inoue, A.; Ishitani, R.; Takagi, J.; Aoki, J.; Nureki, O.

Crystal structure of autotaxin an insight into GPCR activation by lipid mediators. *Nat. Struct. Mol. Biol.* **2011**, *18*, 205-213.

(19) (a) Moeller, A.; Ask, K.; Warburton, D.; Gauldie, J.; Kolb, M. The bleomycin animal model: a useful tool to investigate treatment options for idiopathic pulmonary fibrosis? *Int. J. Biochem. Cell. Biol.* **2008**, *40*, 362-382. (b) Peng, R.; Sridhar, S.; Tyagi, G.; Phillips, J. E.; Garrido, R.; Harris, P.; Burns, L.; Renteria, L.; Woods, J.; Chen, L.; Allard, J.; Ravindran, P.; Bitter, H.; Liang, Z.; Hogaboam, C. M.; Kitson, C.; Budd, D. C.; Fine, J. S.; Bauer, C. M.; Stevenson, C. S. Bleomycin induces molecular changes directly relevant to idiopathic pulmonary fibrosis: a model for "active" disease. *PLoS ONE* [Online] **2013**, *8(4)*, e59348. DOI: 10.1371/journal.pone.0059348.

(20) Noble, P. W.; Albera, C.; Bradford, W. Z.; Costabel, U.; Glassberg, M. K.; Kardatzke, D.; King, T. E. Jr; Lancaster, L.; Sahn, S. A.; Szwarcberg, J.; Valeyre, D.; du Bois, R. M.; CAPACITY Study Group. Pirfenidone in patients with idiopathic pulmonary fibrosis (CAPACITY): two randomised trials. *Lancet.* **2011**, *377*, 1760-1769.

(21) (a) Ashcroft, T.; Simpson, J. M.; Timbrell, V. Simple method of estimating severity of pulmonary fibrosis on a numerical scale. *J. Clin. Pathol.* **1988**, *41*, 467-470. (b) Matsuse, T.; Teramoto, S.; Katayama, H.; Sudo, E.; Ekimoto, H.; Mitsuhashi, H.; Uejima, Y.; Fukuchi, Y.; Ouchi, Y. ICAM-1 mediates lung leukocyte recruitment but not pulmonary fibrosis in a murine model of bleomycin-induced lung injury. *Eur. Respir. J.* **1999**, *13*, 71-77.

(22) This result will be further discussed in a future pharmacology publication. It contradicts observations made with another autotaxin inhibitor in the following article: Black, K. E.; Berdyshev, E.; Bain, G.; Castelino, F. V.; Shea, B. S.; Probst, C. K.; Fontaine, B. A.; Bronova,

I.; Goulet, L.; Lagares, D.; Ahluwalia, N.; Knipe, R. S.; Natarajan, V.; Tager, A. M. Autotaxin activity increases locally following lung injury, but is not required for pulmonary lysophosphatidic acid production or fibrosis. *FASEB J.* **2016**, *30*, 2435-2450.

Table of Contents Graphics

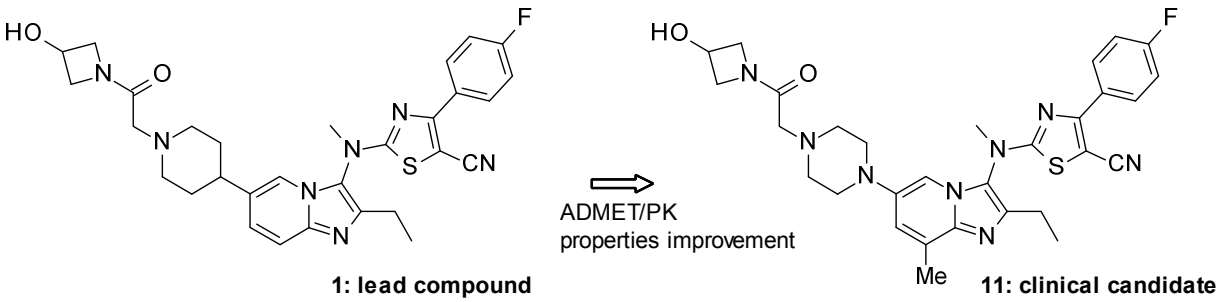

1: lead compound
hERG IC_{50} = 2.9 μM
CYP3A4 TDI positive

11: clinical candidate
hERG IC_{50} = 15 μM
CYP3A4 TDI negative